Deconvoluted methylation profiles discriminate between closely related melanocytic nevi

Daniel Aldea[1], Nicolas Macagno[1,2], Elise Marechal[1], Mathias Moreno[1], Pauline Romanet[1,3], Morgane Pertuit[3], Jérémy Garcia[2], Nathalie Degardin[4], Stéphanie Mallet[5], Isabelle James[6], Guillaume Captier[7], Anne Barlier[1,3], Heather C. Etchevers*[1]

[1] MMG, INSERM, U1251, MarMaRa Institute, Aix Marseille Univ, Marseille, France

[2] Dept. of Pathology, BioGénoPôle, La Timone Hospital, APHM, Marseille, France

[3] Dept. of Molecular Biology, BioGénoPôle, La Timone Hospital, APHM, Marseille, France

[4] Dept. of Pediatric Plastic Surgery, La Timone Hospital, APHM, Marseille, France

[5] Dept. of Dermatology, Venereology and Oncodermatology, La Timone Hospital, APHM, Marseille, France

[6] Clinique du Val de l'Ouest, 69130 Écully, France

[7] Laboratoire d'Anatomie, Dept. of Pediatric Surgery, Montpellier Univ Hospital, University of Montpellier, Montpellier, France

*Corresponding author: Heather C. Etchevers

Email: heather.etchevers@inserm.fr

SUMMARY

Congenital melanocytic nevi (CMN) and common acquired melanocytic nevi (AMN) are melanoma-predisposing skin conditions presenting excessive numbers of melanocytes but arising at different times in life. Appropriately weighted whole-genome methylation analysis can be used as a basis for further research in dermatopathology and as applied here provides new insights into nevus biology.

TO THE EDITOR:

Common or "acquired" (AMN) and congenital melanocytic nevi (CMN) are discrete accumulations of skin melanocytes distinguished by their visibility and size at birth. Both are benign but exhibit differences in presumed origin, phenotype, and implications for human health (reviewed in Maher et al. 2023). AMN emerge as small (<6 mm) postnatal lesions, increasing in number during adolescence to stabilize again in adulthood. In contrast, CMN arise during fetal development. They vary in size, inversely proportional to incidence, from frequent and small (less than 1.5 cm diameter) to rare and giant (exceeding 40 cm). CMN are also diverse in terms of coarse terminal hair, texture, pigmentation dynamics, or nodules, not typical of AMN.

Malignant transformation of any nevus is rare; however, a quarter of all superficial spreading melanomas (SSM) originate from a pre-existing AMN (Pampena et al. 2023). In contrast, multiple medium to giant CMN are associated with significantly increased risk for prepubertal melanoma, particularly nodular (NM) but also extracutaneous, in direct proportion to the size and number of congenital lesions. While many studies focus on transformation of common nevi to melanoma, less is known about the molecular specificities of CMN and how these impact melanoma risk (Bastian et al. 2002).

AMN and CMN are associated with mosaicism for activating mutations at successive levels of the RAS-Mitogen activated protein kinase (MAPK) signaling pathway, which foster melanogenesis. The second most commonly identified somatic mutation in large and giant (L/G) CMN after *NRAS* p.Q61(K/R/L) (Dessars et al. 2009), *BRAF* p.V600E predominates in small CMN and AMN (Muse et al. 2022; Zalaudek et al. 2011). CMN-associated proliferative nodules or melanoma differ in histone H3K27 trimethylation (Busam et al. 2017; Macagno et al. 2018) and propensity to chromosomal breaks (Bastian et al. 2002). While direct epigenetic marks like

DNA methylation may reflect differential nevus potential by exerting stable effects on transcriptional regulation, they had not been studied in confirmed CMN.

We therefore isolated DNA from the CMN of eleven patients scheduled for excision after written, informed consent from their parents (details are in the Supplementary Material and Methods and Supplementary Table S1). Six harbored *NRAS* missense mutations at p.Q61(K or R), one at p.G13R, and four in *BRAF* at p.V600(E). DNA methylation status was assessed using Infinium MethylationEPIC microarrays and integrated with data from eleven patients of a comparable study matching sixteen AMN with adjacent, unaffected control skin samples (Muse et al. 2022). In total, 43 samples were pooled for further analyses. Their clinical and molecular features are compared in Supplementary Table S1.

To account for clinical and cellular variability, we performed reference-based deconvolution of each methylome by predicting proportions of melanocytes, epidermal keratinocytes, and fibroblasts relative to cell-specific methylation profiles (Muse et al. 2022). After normalization, 603,202 5′-C-phosphate-G-3′ (CpG) probes shared a cross-sample bimodal density distribution of beta values (Figure 1a, Supplementary Fig. S1a). Predicted melanocyte proportions in CMN were 55.8% (S.D. ±17.6%), compared to 21.8% (S.D. ±14.6%) in AMN and 7.8% (S.D. ±2.7%) in control skin samples (Figure 1b) (Supplementary Data: Supplementary Fig. S1b). We next measured true proportions of $SOX10^{+}$ melanocytes and $P63^{+}$ keratinocytes in typical CMN (patients 8, 9 and 11) sections adjacent to those used for DNA extraction, quantifying positive immunohistochemistry relative to the pan-cellular expression of $SMARCB1^{+}$ (INI1) in 93153, 194044, or 72000 nuclei, respectively (Figure 1c-d, Supplementary Tables S1-2; Supplementary Fig. S1c). Enumerated by machine learning in an

adaptable workflow (Supplementary Methods), these unbiased measurements validated our methylome-based predictions (Pearson correlation coefficient > 0.95) (Supplementary Fig. S1c).

AMN methylomes are globally hyper-methylated relative to adjacent control skin (Muse et al. 2022), which we confirmed after deconvolution. However, CMN showed more DNA methylome variance, reflecting their inherent heterogeneity (Muse et al. 2022). Deconvoluted CMN profiles were thus not significantly different overall from either AMN or unaffected skin (Figure 1g), prompting closer examination of most differentially methylated positions (DMPs). Pairwise CMN, AMN, and control skin group comparisons pinpointed 51 significant DMPs (Supplementary Table S3). Nearly two-thirds of the DMPs between CMN and control skin were located in intergenic and promoter genomic regions (Figure 1f). Differential methylation of regulatory regions may thus distinguish CMN from AMN or unaffected skin.

Among significantly hypo-methylated CpGs in promoters between CMN and AMN (Figure 1g), the *SPTBN1* gene had two hypo-methylated DMPs (cg07850967 and cg04652957) close to each other and an alternative first exon (Figure 2a-c, Supplementary Table S3). *PAMR1*, *PRR15* and *MIR375* also featured hypo-methylated promoter CpGs (Supplementary Fig. S1e-f and Supplementary Table S3). Consistently, all were previously identified as hyper-methylated in AMN relative to control skin after deconvolution (Muse et al. 2022). Spectrin Beta, Non-Erythrocytic 1 (*SPTBN1*) encodes a key subunit of a tetrameric cytoskeletal protein with homology to α-actinin, involved in cell cycle progression, differentiation, tumor suppression and epithelial maintenance in diverse models (Yang et al. 2021). Intense SPTBN1 immunofluorescence labeled spinous and granular epidermis of all skin samples (Figure 2d-e and Supplementary Fig. S2a-b). SPTBN1 also co-localized with $SOX10^{+}$ basal epidermal melanocytes (Figure 2d-e), concordant with a described role in clustering early perinuclear

melanosomes during maturation (Watabe et al. 2008). Furthermore, SPTBN1 was strongly expressed in SOX10^{+} dermal melanocytes of CMN, compared to weaker fibroblast or junctional melanocyte staining in AMN (Figure 2d-e and Supplementary Fig. S2a-b).

Genome methylation in distinct subtypes of melanocytic nevi does not differ globally, after accounting for the inter- and interlesional heterogeneity of CMN. Deconvolution can strengthen the signals of specific differentially methylated loci potentially impacting expression, as the example of CMN beta-spectrin. By demonstrating fruitful integration of new with existing repository datasets, this approach enables further discoveries of functionally relevant CpGs with additional cohorts in the future.

DATA AVAILABILITY STATEMENT

Datasets related to this article can be found at [https://doi.org/10.6084/m9.figshare.26005255.v1], hosted at figshare. Methylome data for AMN and control skin are available at GEO under accession GSE188593 (Muse et al. 2022). Methylome data for CMN are available at GEO under accession GSE268769 or released to qualified investigators upon request to the authors. All other data are available in the manuscript or the supplementary materials.

ORCIDs

Daniel Aldea 0000-0001-5101-0194
Nicolas Macagno 0000-0002-9882-2162
Elise Marechal 0000-0003-4586-3304
Mathias Moreno 0000-0002-7057-0063
Pauline Romanet 0000-0003-1775-9569
Morgane Pertuit 0009-0003-9958-7496
Jeremy Garcia 0000-0001-9432-3529
Nathalie Degardin 0000-0003-3625-7687
Stéphanie Mallet 0000-0003-2884-0645
Isabelle James 0000-0002-9485-7421
Guillaume Captier 0000-0002-1705-2339
Anne Barlier 0000-0002-3740-6173
Heather Etchevers 0000-0003-0201-3799

Conflict of interest: The authors state no conflict of interest.

ACKNOWLEDGMENTS

The authors thank the many patients who agreed to take part in this study. This work was supported by the Horizon Europe Mission Cancer grant 101096667 MELCAYA, the AFM-Téléthon strategic project MoThARD, with additional grants from Nevus Outreach, Inc. (USA), Asociación Española de Afectados por Nevus Gigante Congénito (Spain), Association du

Naevus Géant Congénital (France), Institut MarMaRa of Aix-Marseille Université, (France) and Naevus 2000 France-Europe (France).

AUTHOR CONTRIBUTIONS STATEMENT (CRediT-compliant):

N.M. and H.C.E.: **Conceptualization**, **Supervision**. D.A., N.M., E.M. and J.G.: **Investigation**. E.M., D.A., and H.C.E.: **Writing – Original Draft**. D.A., N.M., P.R.: **Methodology**. E.M., M.M., and M.P.: **Validation**. D.A., N.M. J.G.: **Formal analysis**. N.D., S.M., I.J. and G.C.: **Resources** (patient enrollment & consent). D. A. and H.C.E.: **Visualization** N.M., A.B. and H.C.E.: **Writing – Reviewing and Editing**; **Funding Acquisition**. H.C.E.: **Project administration**.

REFERENCES

Bastian BC, Xiong J, Frieden IJ, Williams ML, Chou P, Busam K, et al. Genetic changes in neoplasms arising in congenital melanocytic nevi: differences between nodular proliferations and melanomas. The American Journal of Pathology. 2002;161(4):1163–9

Busam KJ, Shah KN, Gerami P, Sitzman T, Jungbluth AA, Kinsler V. Reduced H3K27me3 Expression is Common in Nodular Melanomas of Childhood Associated with Congenital Melanocytic Nevi but Not in Proliferative Nodules. American Journal of Surgical Pathology. 2017;41(3):396–404

Dessars B, De Raeve LE, Morandini R, Lefort A, El Housni H, Ghanem GE, et al. Genotypic and Gene Expression Studies in Congenital Melanocytic Nevi: Insight into Initial Steps of Melanotumorigenesis. Journal of Investigative Dermatology. 2009;129(1):139–47

Macagno N, Etchevers HC, Malissen N, Rome A, Hesse S, Mallet S, et al. Reduced H3K27me3 Expression is Common in Nodular Melanomas of Childhood Associated With Congenital Melanocytic Nevi But Not in Proliferative Nodules. Am. J. Surg. Pathol. 2018;42(5):701–4

Maher NG, Scolyer RA, Colebatch AJ. Biology and genetics of acquired and congenital melanocytic naevi. Pathology. 2023;55(2):169–77

Muse ME, Bergman DT, Salas LA, Tom LN, Tan J-M, Laino A, et al. Genome-Scale DNA Methylation Analysis Identifies Repeat Element Alterations that Modulate the Genomic Stability of Melanocytic Nevi. J Invest Dermatol. 2022;142(7):1893-1902.e7

Pampena R, Piccolo V, Muscianese M, Kyrgidis A, Lai M, Russo T, et al. Melanoma in children: A systematic review and individual patient meta-analysis. Journal of the European Academy of Dermatology and Venereology. 2023;37(9):1758–76

Watabe H, Valencia JC, Le Pape E, Yamaguchi Y, Nakamura M, Rouzaud F, et al. Involvement of Dynein and Spectrin with Early Melanosome Transport and Melanosomal Protein Trafficking. J Invest Dermatol. 2008;128(1):162–74

Yang P, Yang Y, Sun P, Tian Y, Gao F, Wang C, et al. βII spectrin (SPTBN1): biological function and clinical potential in cancer and other diseases. International Journal of Biological Sciences. 2021;17(1):32–49

Zalaudek I, Guelly C, Pellacani G, Hofmann-Wellenhof R, Trajanoski S, Kittler H, et al. The Dermoscopical and Histopathological Patterns of Nevi Correlate with the Frequency of BRAF Mutations. J Invest Dermatol. 2011;131(2):542–5

FIGURE LEGENDS

Figure 1.

Inferred cellular architecture of congenital melanocytic nevi and epigenetic methylation in CMN vs. AMN. **(a)** Density plots of quantile-normalized and cell-deconvoluted beta values from CMN, AMN, and control Skin groups. **(b)** Estimated cellular proportions in congenital or acquired melanocytic nevi (CMN and AMN), versus control skin (Skin) for melanocytes (Mel), keratinocytes (Ker), and fibroblasts (Fib). Each vertical line represents one sample (N=43 samples). For AMN and Skin, samples from the same patient are underlined. AMN and unaffected Skin data were obtained from the Gene Expression Omnibus accession GSE188593 (Muse et al. 2022). **(c)** Representative CMN images. Hematoxylin-phloxine-saffron (HPS) staining shows high nuclear density (purple) underlying the epidermis. Immunohistochemistry staining of SOX10 for (nevo)melanocytes, P63 for epidermis and epidermal annexes, and SMARCB1 for all normal nuclei. The epidermal-dermal junction is delimited by dotted lines. Melanocytic nests (black arrow) are indicated. **(d)** Boxplot showing true *versus* estimated cellular proportions of $SOX10^+$ melanocytes and $P63^+$ keratinocytes in CMN, N=3 independent samples (patients 8, 9, 11). **(e)** Box plots representing global DNA methylation of CMN, AMN, and unaffected Skin. The mean of beta values across 603,202 CpG probes common to all samples is plotted. **(f)** The genomic distribution of the hyper- and hypo-methylated DMPs is classified into 3 genomic locations; body gene, intergenic, and promoter (1500-TSS, 200-TSS, 5'UTR). **(g)** Top hypo-methylated DMPs in CMN vs AMN within the promoter region. Significance was assessed by **(d)** a two-tailed Mann-Whitney T-test and **(e)** Kruskal-Wallis one-way ANOVA. ns. not significant, ***P<0.001.

Figure 2.

Spectrin Beta, non-erythrocytic 1 (SPTBN1), a general marker of nevomelanocytes. (a) DMP genomic positions within the *Spectrin Beta, Non-Erythrocytic 1* (*SPTBN1*) locus. **(c)** Box-plot of the β-values of two DMPs within the *SPTBN1* promoter region. **(d-e)** Representative images of CMN, and AMN stained with antibodies against SPTBN1 (purple) and SOX10 (white), a known melanocyte marker of the superficial skin. Dermal and epidermal melanocytes are indicated by yellow arrows or white double arrowheads, respectively. The dermal-epidermal junction is denoted by dotted lines, nuclei stained by DAPI. Scale bar = 100 µm. In **(c),** significance was assessed by a Kruskal-Wallis one-way ANOVA. n.s. not significant, **P<0.01, ****P<0.0001.

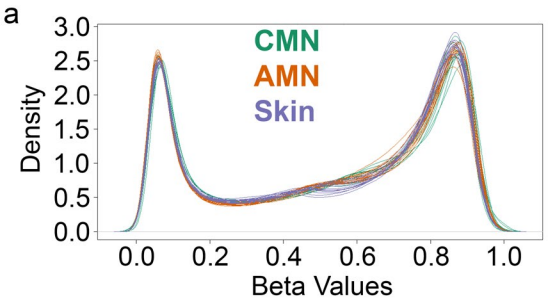

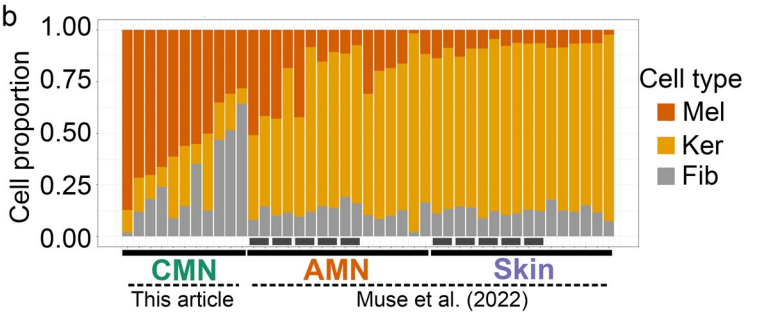

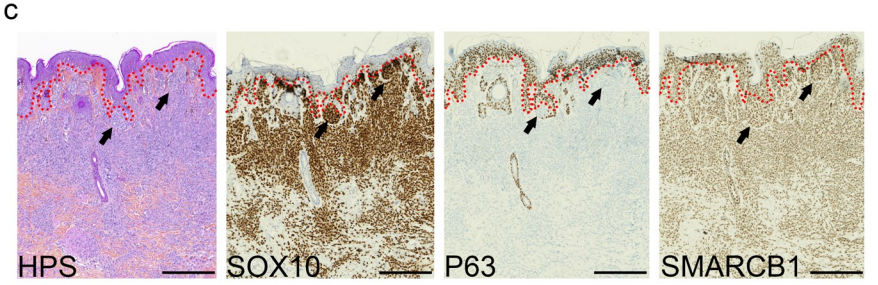

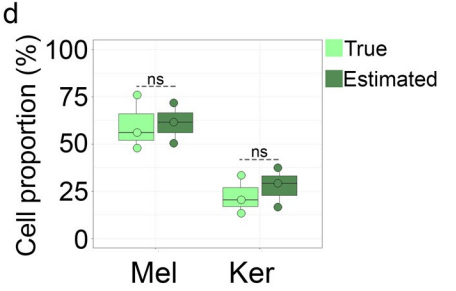

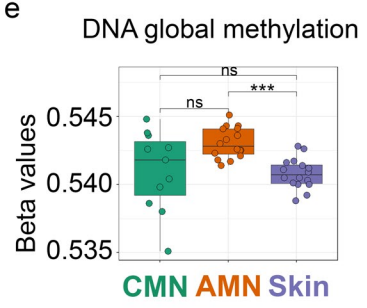

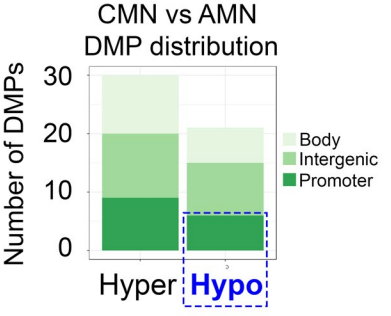

g

Top hypo-methylated DMPs within putative promoters

Associated genes	Probe names
SPTBN1	cg07850967, cg04652957
CRISPLD2	cg03296797
BCAS3	cg03821916
CSGALNACT1	cg05800416
CLDN9	cg08199758

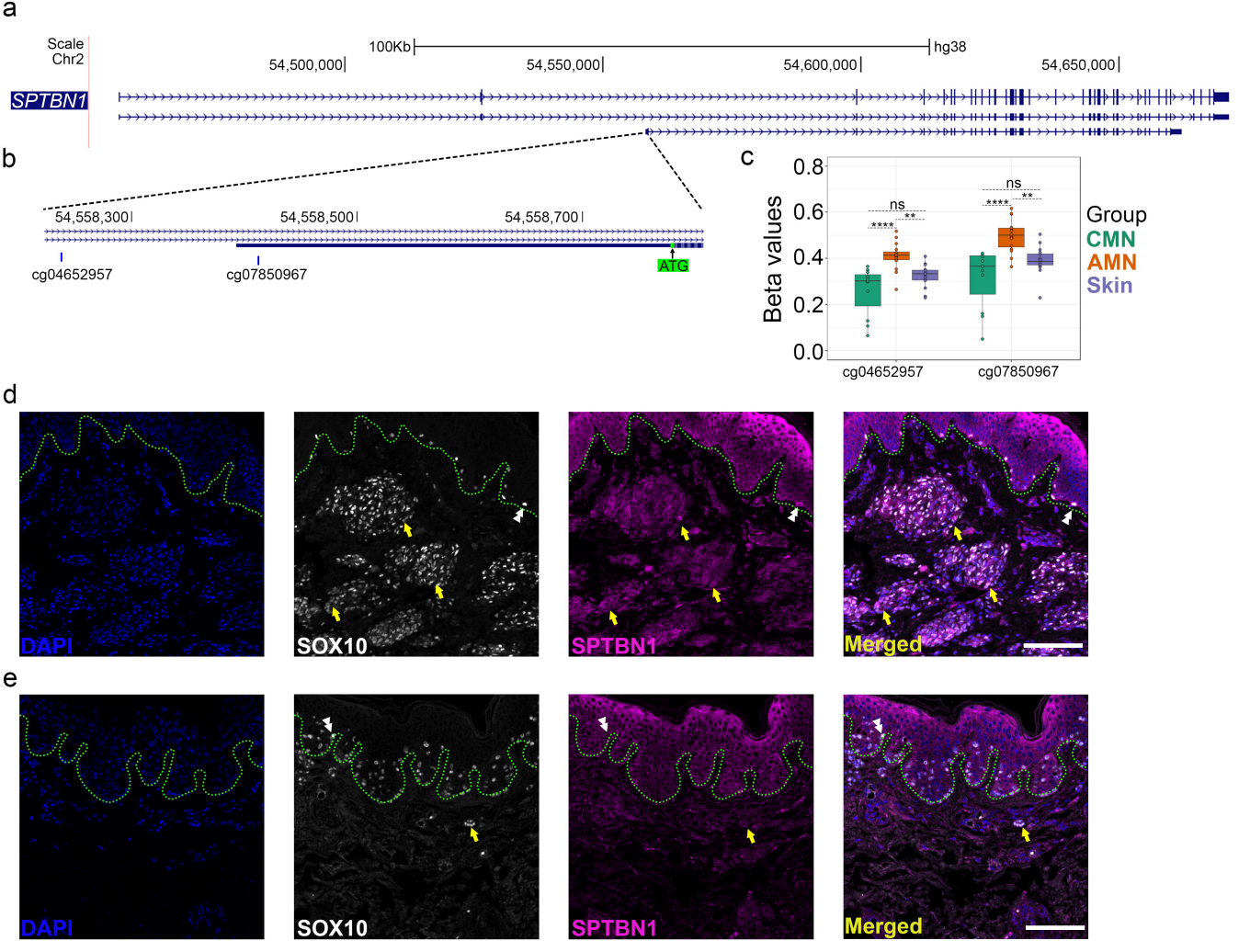
a
Scale
Chr2
100Kb
hg38
54,500,000
54,550,000
54,600,000
54,650,000
SPTBN1
b
54,558,300
54,558,500
54,558,700
cg04652957
cg07850967
ATG
c
Beta values
0.8
0.6
0.4
0.2
0.0
ns
****
**
Group
CMN
AMN
Skin
cg04652957
cg07850967
d
DAPI
SOX10
SPTBN1
Merged
e
DAPI
SOX10
SPTBN1
Merged